Morphology Controllable Synthesis of α-Fe_2O_3 1D Nanostructures: Growth Mechanism and Nanodevice Based on Single Nanowire

L. Liao,[†] Z. Zheng,[†] B. Yan,[†] J. X. Zhang,[‡] H. Gong,[‡] J. C. Li,[§] C. Liu,[§] Z. X. Shen,[†] and T. Yu*,[†]

Division of Physics and Applied Physics, School of Physical and Mathematical Sciences, Nanyang Technological University, Singapore 637616, Department of Materials Science and Engineering, National University of Singapore, Blk E3A, 7 Engineering Drive 1, Singapore 117576, Key Laboratory of Acoustic and Photonic Materials and Devices of Ministry of Educations, Department of Physics, Wuhan University, Wuhan 430072, China

Received: April 6, 2008; Revised Manuscript Received: May 5, 2008

Single crystalline α-Fe_2O_3 nanoflakes and nanowires are controllably synthesized simply by heating iron foil at different temperatures. The growth mechanisms are proposed based on the electron microscopy results. Electrical transport studies reveal *n*-type semiconducting behavior of α-Fe_2O_3 nanowire. A new type of α-Fe_2O_3 gas sensor based on single α-Fe_2O_3 nanowire as sensing unit is developed. The gas sensing on electron transport through the nanowire is investigated. Moreover, the CO detection sensitivity can be modulated by the gate voltage. Our results indicate that α-Fe_2O_3 nanowire holds good potential for nanoscale sensing applications.

1. Introduction

Sensing of poisonous gas is very important for saving human lives and preserving industrial safety. In order to improve the integration, sensitivity, selectivity, and chemical and thermal stability of the poisonous gas detectors, intensive efforts have been afforded in developing gas sensors based on nanostructured materials, such as carbon nanotubes,[1] metal oxide nanoparticles,[2] and nanowires.[3]

Several semiconducting oxides such as SnO_2, ZnO, α-Fe_2O_3, and In_2O_3 have been employed as gas sensors, by utilizing the change of the electrical conductivity of these materials upon exposing to target gases.[4–6] α-Fe_2O_3, which is the most stable iron oxide under ambient conditions, exhibits a rhombohedral structure with indirect band gap of 2.1 eV.[7] In recent years, various α-Fe_2O_3 nanostructures have been studied, including their shape-specific properties, synthesis methods,[8–11] and potential applications on lithium ion battery electrodes,[12] gas sensors,[9] field effect transistor,[13,14] catalysts,[15] and field emission.[11] α-Fe_2O_3 has long been used in gas sensing applications, for example detecting gases like H_2,[16] ethanol,[16] NO_2,[17] CO,[17] H_2S,[18,19] and CH_3OH.[20] Nanowires are considered as ideal building blocks for constructing nanosized devices due to their high surface to volume ratio and their special physical and chemical properties resulting from the reduced sizes. However, few studies focus on gas sensors based on a single α-Fe_2O_3 nanostructure.

In this paper, α-Fe_2O_3 nanostructures were prepared by heating Fe foil in a box oven. The morphologies of the products could be effectively controlled either as nanoflakes or nanowires by altering the growth temperature. The nanostructures obtained are *n*-type semiconductor. Nanodevices based on a single α-Fe_2O_3 nanowire such as field effect transistor and gas sensor were developed. The α-Fe_2O_3 nanowire based gas sensor has fast response and high sensitive to reductive gases in air at room temperature. This work is a continuation of our ongoing efforts toward the nanodevice of transition metal oxide nanostructures.[21,22]

2. Experimental Section

2.1. Synthesis and Characterization. Fresh iron foils (10 × 10 × 0.1 mm) with a purity of 99.9% (Aldrich) were used as both reagents and substrates for the growth of α-Fe_2O_3 nanostructures. The cleaned Fe foil was heated in a box oven under ambient conditions. The growth temperature was varied between 300−800 °C, while the heating duration was fixed at 10 h.

The microstructures and morphology of α-Fe_2O_3 nanostructures were characterized by X-ray diffraction (XRD, D8 Advanced) and scanning electron microscopy (SEM, JEOL JSM-6700F). Transmission electron microscopy (TEM) was performed using a 200 kV JEOL 2010F field-emission-gun. A Raith electron-beam lithography system was used to fabricate the Au electrodes.

2.2. Fabrication and Measurement of Nanodevice. The as-grown α-Fe_2O_3 nanowires were dispersed on SiO_2/Si substrate. The thickness of the thermally grown SiO_2 layer was 200 nm. A photoresist layer of SU-8 was subsequently spun over the SiO_2/Si substrate. Two electrical contact fingers together with their bonding pads were exposed by electron-beam lithography. After the development, a 200-nm thick Au film was deposited over the structure and followed by a lift-off process.

Gas sensing properties of the samples were examined at room temperature. The testing gases were pure air and 50−400 ppm CO gas in air. The gas sensing response of the nanodevice was defined as the ratio of the electrical resistance in air (R_a) to that in testing gas (R_g). The sample resistance as a function of time was measured by using a Keithley 4200 SCS semiconductor characterization system.[21]

3. Results and Discussion

A low-magnification SEM image (Figure 1) shows the α-Fe_2O_3 nanostructures on the Fe foil substrate. The α-Fe_2O_3

* To whom correspondence should be addressed. Tel: +65-6316-7899. E-mail: Yuting@ntu.edu.sg. URL: www.ntu.edu.sg/home/yuting/.
[†] Nanyang Technological University.
[‡] National University of Singapore.
[§] Wuhan University.

10.1021/jp802968a CCC: $40.75
Published on Web 06/26/2008

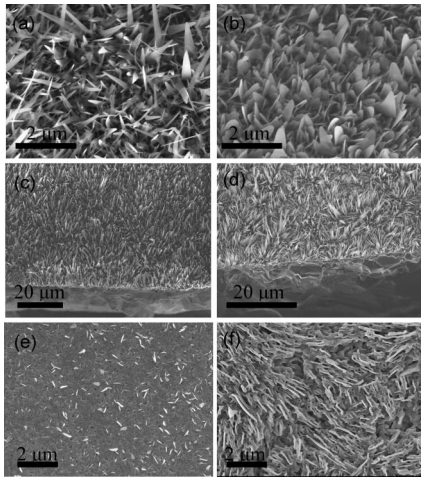

Figure 1. SEM images of α-Fe_2O_3 nanostructures on Fe foils after heating it at (a) 300, (b) 400, (c) 750, (d) 800, (e) 500, and (f) 900 °C for 10 h.

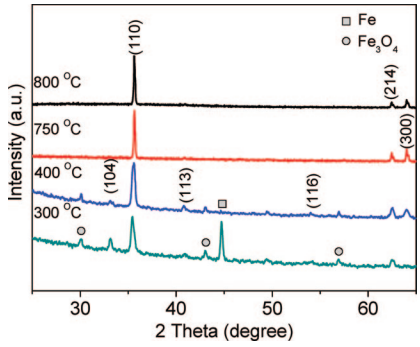

Figure 2. XRD patterns of α-Fe_2O_3 nanostructures on Fe foils after heating it at (a) 300, (b) 400, (c) 750, and (d) 800 °C.

nanoflakes were obtained by annealing the Fe foil at 300−400 °C, whereas the α-Fe_2O_3 nanowires could be obtained when the heating temperature was raised to 750−800 °C. Clearly, the nanoflakes become broader with increasing reaction temperature, indicating the obvious heating temperature's effect on the morphologies of the nanostructures. In general, the random aligned nanoflakes synthesized at the low temperature are about 5−20 nm in thickness, 5−10 nm at the tips, and 1−2 μm in length. The vertical aligned α-Fe_2O_3 nanowires fabricated at higher temperatures were about 10 μm in length, and about 100 nm in diameter. It is noted that neither nanoflakes nor nanowires are able to be synthesized when the heating temperature is within the range of 400−750 °C or above 800 °C (as shown in Figure 1, panels e and f). The proposed explanation could be found in the growth mechanism discussion below.

Figure 2 displays the XRD patterns of the samples. As can be seen, two phases of iron oxide, α-Fe_2O_3 and Fe_3O_4, are present in the low-temperature synthesized samples. However, when the growth temperature is raised to 750−800 °C, the samples show pure α-Fe_2O_3 phase (rhombohedral structure). Furthermore, the (110) peak at 35.2° is dominant, indicating that the α-Fe_2O_3 nanowires grow along the [110] direction; that is, the growth axis is along the *c* direction.[10]

Figure 3a shows the typical TEM image of α-Fe_2O_3 nanoflakes. As can be seen in the high resolution TEM (HRTEM) image (Figure 3b) of the region taken from Figure 3a, the fringe spacing of 0.25 nm concurs well with the interplanar spacing of the plane (110). The TEM image of an individual α-Fe_2O_3 nanowire is shown in Figure 3c. The selected area electron diffraction (SAED) pattern of the nanowire is shown as inset

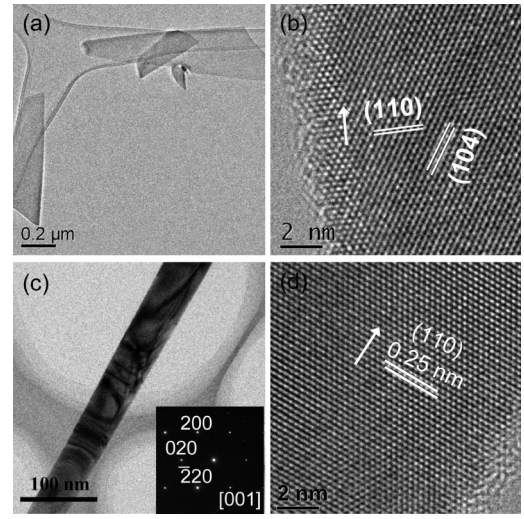

Figure 3. (a) TEM and (b) HRTEM images of a single α-Fe_2O_3 nanoflake, (c) TEM, and (d) HRTEM image of a single α-Fe_2O_3 nanowire. Inset of panel c shows the SAED pattern.

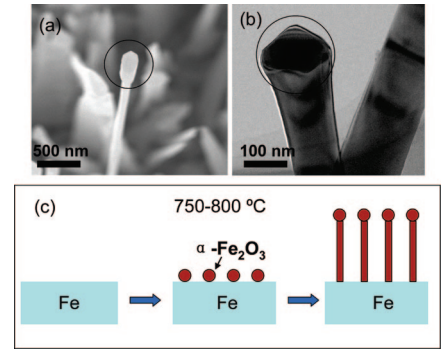

Figure 4. SEM (a) and TEM (b) images of the catalyst of a single α-Fe_2O_3 nanowire. (c) A schematic diagram of the formation and growth of α-Fe_2O_3 nanowires.

of Figure 3c. The growth direction of the nanowire was [110], which is consistent with the previous study.[23]A typical HRTEM pattern (Figure 3d) taken from the nanowire in Figure 3c confirms that the nanowire is single crystalline. The spacing (0.25 nm) between adjacent lattice planes corresponds to the distance between adjacent (110) planes, showing again that the orientation of *c*-axis is the growth direction of the α-Fe_2O_3 nanowires.

Based on our present study, the growth mechanism of α-Fe_2O_3 nanostructures was proposed as below. Considering the growth temperature (300−400 °C) is much lower than the saturation vapor pressure point of Fe (above 700 °C),[24] the growth of α-Fe_2O_3 nanoflakes is inexplicable by the vapor phase mechanism such as the vapor−liquid−solid (VLS) and vapor−solid (VS) processes. In our previous work, we attributed the growth mechanism of α-Fe_2O_3 nanoflakes to the surface diffusion of iron atoms and iron oxide molecules, driven by the oxygen rich and iron deficient along the [110] direction.[25] However, when the growth temperature is up to 750 °C, the Fe foil starts vaporizing and a little amount of iron vapor (vapor pressure $<1 \times 10^{-8}$ Pa) could be generated, which may source the continuous growth of nanowires. Catalysts on the top of α-Fe_2O_3 nanowires were clearly observed in the SEM and the TEM images (Figure 4, panels a and b). As there is no foreign metal, self-catalyst vapor-solid (VS) process is proposed in this work. The relative high temperatures may also facilitate structure reorganization from a flake to a cylindrical structure so as to

minimize the surface energy. A schematic view of the formation of the α-Fe_2O_3 nanowire is shown in Figure 4c. First, the top layer of Fe foil was oxidized directly by the oxygen molecules in air and formed a very thin layer of α-Fe_2O_3 nanocrystals as catalysts. Then, α-Fe_2O_3 vapor was generated by oxidizing the Fe vapor molecular or directly vaporizing the thin top oxide layer. The relatively low pressure of α-Fe_2O_3 vapor resulted from the low vapor pressure of Fe and slow rate of formation of α-Fe_2O_3 vapor in the reaction chamber ensure the growth of low dimensional, in this work wire-like nanostructures.[26] Within the temperature range of 400−750 °C, instead of nanoflakes or nanowires, a relatively dense α-Fe_2O_3 film was formed on the top of the substrate Fe foil. This gap could be explained by the fact that the energy is high enough to facilitate surface diffusion in all directions and results in the formation of nanoparticles. However, the heating temperature is lower than the vapor point of Fe, and consequently, there are not enough sources for triggering the growth of nanowires. Likewise, when the temperature is above 800 °C, the worm-like structures are formed on the surface shown in Figure 1f, because the vapor pressure might be too high and causes the three-dimensional growth.

For future applications, we fabricated the nanodevices based on a single α-Fe_2O_3 nanowire. The schematic diagram of configuration and SEM image of a single α-Fe_2O_3 nanowire field effect transistor is shown in Figure 5, panels a and b. Figure 5c displays the $I_{ds}-V_{ds}$ curves of the nanodevice. From the $I_{ds}-V_{ds}$ curves obtained under gate voltages (V_{gt}) of −20, −10, 0, 20, and 40 V, it can be clearly seen that the conductance of the nanowire increases monotonically as the gate potential increases. The *n*A current level reveals low conductivity of the nanowires. Figure 5d shows the $I_{ds}-V_{gt}$ curve of the nanowire field effect transistor. As known, the electron carrier concentration (n) and field effect mobility (μ) in a typical cylindrical nanowire system with radius r can be expressed as[13,14]

$$n = \frac{V_{gt}}{e}\frac{2\pi\varepsilon_0\varepsilon_r}{\ln(2h/r)} \quad (1)$$

$$\mu = \frac{dI}{dV_g}\frac{\ln(2h/r)}{2\pi\varepsilon_0\varepsilon_r}\frac{L}{V_{ds}} \quad (2)$$

where V_{gt} is the threshold gate voltage, e is the electron charge, ε_r ($\varepsilon_r = 3.9$ for SiO_2) is the relative dielectric constant, h is the thickness of gate oxide layer, and L is the channel length. Because a nanowire has a cylindrical geometry, it is reasonable to estimate the capacitance using $a = 2r$ as a first order approximation. $V_{gt} = -20$ V and $dI/dV_{gt} = 2.6 \times 10^{-10}$ A/V can be extrapolated from the linear region (−10 to +40 V) of $I_{ds}-V_{gt}$ curve. Therefore, the electron concentration is estimated to be $n = 1.29 \times 10^8$ cm^{-1}, which corresponds to a bulk concentration of 1.48×10^{18} cm^{-3}, and the mobility is calculated to be $\mu_e = 1.79 \times 10^{-1}$ cm^2/V s, which demonstrate their *n*-type semiconducting behavior.

Figure 6a is the corresponding *S*/*t* (sensitivity vs time) curve of a single α-Fe_2O_3 nanowire gas sensor subjected to CO gas with various concentrations at room temperature, where S is defined as the ratio of R_{air} to R_g as described in the experimental section. High CO sensitivity and short response time (less than 10 s) were obviously seen in this work. The α-Fe_2O_3 nanowire sensor has a good sensing performance as compared to other α-Fe_2O_3 nanostructures and film devices as well as metal-oxide bulk material CO sensors at room temperature shown in Table 1.[18,19,27–29] The curve of sensitivities versus CO concentration is shown in Figure 6b where the sensitivity of the sample exhibits nonlinear behavior with CO concentration. The sensitivity increases with increase in the CO gas concentration. In fact, the sensitivity of the semiconducting metal oxide can usually be empirically represented as $S_g = 1 + aP_g^{\beta}$,[30] where a is a constant, and P_g is the target gas partial pressure that is directly proportional to its concentration. The sensitivity is characterized by the prefactor, P_g, and exponent, β.[30] β may have some rational fraction value (usually 1 or 1/2), depending on the charge of the surface species and the stoichiometry of

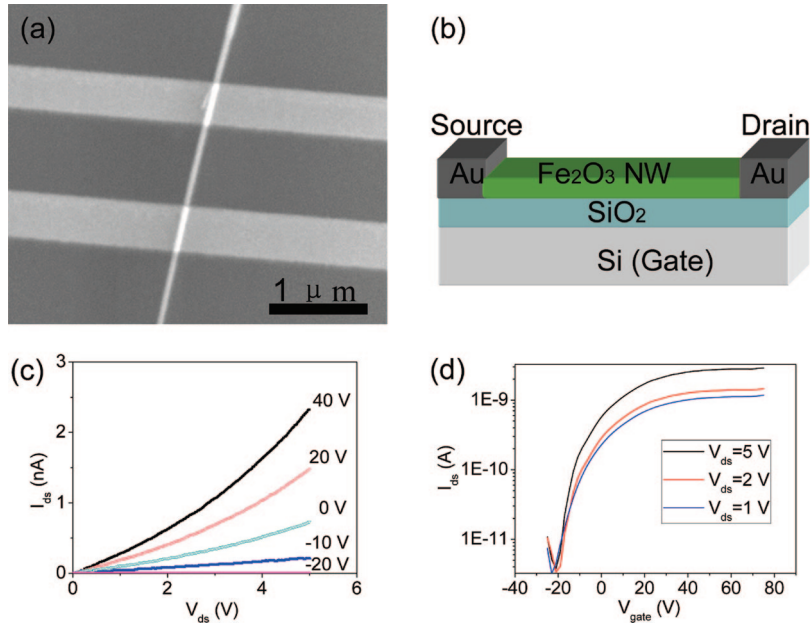

Figure 5. (a) SEM image of a single α-Fe_2O_3 nanowire field effect transistor, (b) the schematic diagram of configuration of a single α-Fe_2O_3 nanowire field effect transistor, (c) $I_{ds}-V_{ds}$ curves of a single α-Fe_2O_3 nanowire field effect transistor, (d) $I_{ds}-V_{gt}$ curves of a single α-Fe_2O_3 nanowire field effect transistor.

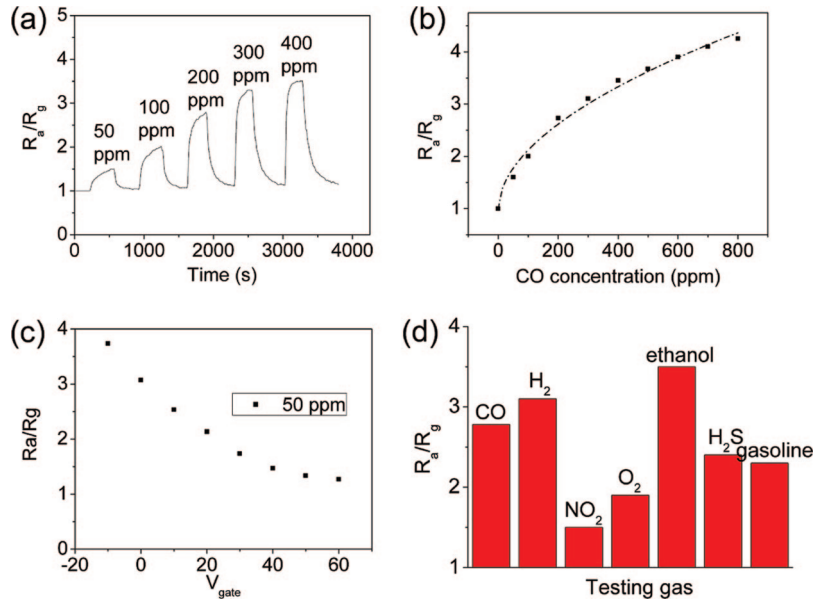

Figure 6. (a) Gas sensibility response curve of a single α-Fe_2O_3 nanowire for different CO concentration, (b) sensitivity vs CO concentration in the range of 50−800 ppm. The dash line represents the theoretical curve of the empirical model, (c) the relationship between sensitivity and gate voltage, and (d) sensitivity of a single α-Fe_2O_3 nanowire sensor for different gases at a fixed concentration of 200 ppm.

TABLE 1: Gas Sensing Properties of Different α-Fe_2O_3 Structures

Fe_2O_3 structures	gas kinds	sensitivity (R_a/R_g)	response time (s)
Pt doped α-Fe_2O_3 thick film[18]	H_2S	about 100	about 100 s
α-Fe_2O_3 nanotubes film[19]	H_2S	about 3−4	about 15 s
α-Fe_2O_3 nanorings film[27]	ethanol	about 400	about 60 s
α-Fe_2O_3 porous nanospheres film[28]	ethanol	more than 10	about 10 s
α-Fe_2O_3 film[29]	ethanol	about 10	about 20 s
single α-Fe_2O_3nanowires in this paper	CO	about 5	less than 10 s

the elementary reactions on the surface. In the case of single α-Fe_2O_3 nanowires device, β was found to be 1/2 with the CO concentration in the range 50−800 ppm. For comparison, a theoretical curve of the empirical model of the gas sensitivity is also shown in Figure 6b. It is found that our measured data show good agreement with the empirical model. Similar results, which are not shown here, have been reproduced for another ten gas nanosensors.

Figure 6c shows the dependence of the sensitivity on the gate voltage for 50 ppm CO. The maximum sensitivity of 3.8 appears at −10 V, which is just above the gate threshold voltages −20 V in 50 ppm CO. The gate dependence of CO detection sensitivity can be attributed to the gate modulation of the electron concentration in the nanowire channel.[23] When the gate voltage is far above the threshold voltage, electron concentration in the nanowire channel is quite high and the CO molecules absorbed on the nanowire surface capture only a small portion of the available electrons. Therefore, the relative conductance change is very small. However, when the nanowire field effect transistor is gated just above the threshold, channel electrons are substantially depleted and the conductance change was caused by CO adsorption becomes much more significant. The above results are reproducible. This effectively demonstrates the advantage of α-Fe_2O_3 nanowire FET as a CO sensor, for example not only offering the large surface-to-volume ratio, but also the increased detection sensitivity at appropriate gate voltages.

We also measured the response of the sensor to other gases at concentration of 200 ppm, such as CO, H_2, ethanol, gasoline, NO_2, O_2, and H_2S under a bias voltage of 5 V. The sensitivity of α-Fe_2O_3 sensor to different gases is shown in Figure 6d. The sensor response to oxidation gas was low with respect to that obtained for reductive gas. The result also proves that the gas sensitivity mechanism is based on the modulation model of the depletion layer.[21,31] The surface of the nanowire absorbs O_2 from air by trapping conductive electrons in α-Fe_2O_3, resulting in a decrease of electron concentration in nanowire and consequently an increase of resistance R_a. The more the absorbed O_2, the higher R_a. After exposing it to CO or other reductive gases, the trapped electron is released to α-Fe_2O_3, which causes the electron concentration of nanowire to increases and R_g decreases.

4. Conclusion

In conclusion, α-Fe_2O_3 nanostructures with various morphologies were prepared by heating metal foil in a box oven at different temperatures. The growth mechanism of nanowires was proposed. The α-Fe_2O_3 nanowire is a typical *n*-type semiconductor. Single α-Fe_2O_3 nanowire-based field effect transistor and gas sensor have been fabricated. Furthermore, the gas sensor based on a single α-Fe_2O_3 nanowire has fast response and high sensitive to CO in air. This new type of gas nanosensor is expected to find wide applications in various complicated gas for quick detection of poisonous and inflammable gases.

References and Notes

(1) Huang, X. J.; Sun, Y. F.; Wang, L. C.; Meng, L. F.; Liu, J. H. *Nanotechnology* **2004**, *15*, 1284.
(2) Ahmad, M. M.; Makhlouf, S. A.; Khalil, K. M. S. *J. Appl. Phys.* **2006**, *100*, 094323.
(3) Cheng, Y.; Xiong, P.; Fields, L.; Zheng, J. P.; Yang, R. S.; Wang, Z. L. *Appl. Phys. Lett.* **2006**, *89*, 093114.
(4) Yoon, D. H.; Choi, G. M. *Sens. Actuators B* **1997**, *45*, 251.

(5) Horrillo, M. C.; Serventi, A.; Rickerby, D.; Gueierrez, J. *Sens. Actuators B* **1999**, *58*, 474.
(6) Papadopoulos, C. A.; Vlachos, D. S.; Avaritsiotis, J. N. *Sens. Actuators B* **1997**, *42*, 95.
(7) Wang, R.; Chen, Y.; Fu, Y.; Zhang, H.; Kisielowski, C. *J. Phys. Chem. B* **2005**, *109*, 12245.
(8) Vayssieres, L.; Sathe, C.; Butorin, S. M.; Shuh, D. K.; Nordgren, J.; Guo, J. H. *Adv. Mater.* **2005**, *17*, 2320.
(9) Woo, K.; Lee, H. J.; Ahn, J. P.; Park, Y. S. *Adv. Mater.* **2003**, *15*, 1761.
(10) Zhu, Y. W.; Yu, T.; Sow, C. H.; Liu, Y. J.; Wee, A. T. S.; Xu, X. J.; Lim, C. T.; Thong, J. T. L. *Appl. Phys. Lett.* **2005**, *87*, 023103.
(11) Yu, T.; Zhu, Y. W.; Xu, X. J.; Yeong, K. S.; Shen, Z. X.; Chen, P.; Lim, C. T.; Thong, J. T.; Sow, C. H. *Small* **2006**, *2*, 80.
(12) Reddy, M. V.; Yu, T.; Sow, C. H.; Shen, Z. X.; Lim, C. T.; Subba Rao, G. V.; Chowdari, B. V. R. *Adv. Funct. Mater.* **2007**, *17*, 2792.
(13) Fan, Z. Y.; Wen, X. G.; Yang, S. H.; Lu, J. G. *Appl. Phys. Lett.* **2005**, *87*, 013113.
(14) Lee, Y. C.; Chueh, Y. L.; Hsieh, C. H.; Chang, M. T.; Chou, L. J.; Wang, Z. L.; Lan, Y. W.; Chen, C. D.; Kurata, H.; Isoda, S. *Small* **2007**, *3*, 1356.
(15) Peng, F.; Fu, X. B.; Yu, H.; Wang, H. J. *Carbon* **2007**, *45*, 1.
(16) Chen, J.; Xu, L. N.; Li, W. Y.; Gou, X. L. *Adv. Mater.* **2005**, *17*, 582.
(17) Neri, G.; Bonavita, A.; Galvagno, S.; Siciliano, P.; Gapone, S. *Sen. Actuators. B* **2002**, *82*, 40.
(18) Wang, Y.; Wang, S. R.; Zhao, Y. Q.; Zhu, B. L.; Kong, F. H.; Wang, D.; Wu, S. H.; Huang, W. P.; Zhang, S. M. *Sen. Actuators. B* **2007**, *125*, 79.
(19) Sun, Z. Y.; Yuan, H. Q.; Liu, Z. M.; Han, B. X.; Zhang, X. R. *Adv. Mater.* **2005**, *17*, 2993.
(20) Wu, C. Z.; Yin, P.; Zhu, X.; Ouyang, C. Z.; Xie, Y. *J. Phys. Chem. B* **2006**, *110*, 17806.
(21) Liao, L.; Lu, H. B.; Li, J. C.; Liu, C.; Fu, D. J.; Liu, Y. L. *Appl. Phys. Lett.* **2007**, *91*, 173110.
(22) Liao, L. Mai, H. X. Yuan, Q. Lu, H. B. Li, J. C. Liu, C. Yan, C. H. Shen, Z. X. and Yu, T. *J. Phys. Chem. C* **2008**, *112,* 9601.
(23) Fu, Y. Y.; Wang, R. M.; Xu, J.; Chen, J.; Yan, Y.; Narlikar, A. V.; Zhang, H. *Chem. Phys. Lett.* **2003**, *379*, 373.
(24) Lide, D. R. *CRC Handbook of Chemsitry and Physics*, 88th ed.; CRC Press: Boca Raton, FL, 2007; pp 4−130.
(25) Zheng, Z.; Chen, Y. Z.; Shen, Z. X.; Ma, J.; Sow, C. H.; Huang, W.; Yu, T. *Appl. Phys. A: Mater. Sci. Process.* **2007**, *89*, 115.
(26) Dai, Z. R.; Pan, Z. W.; Wang, Z. L. *Adv. Fun. Mater.* **2003**, *13*, 9–24.
(27) Hu, X. L.; Yu, J. C.; Gong, J. M.; Li, Q.; Li, G. S. *Adv. Mater.* **2007**, *19*, 2324.
(28) Guo, X. L.; Wang, G. X.; Park, J. S.; Liu, H.; Yang, J. *Nanotechnology* **2008**, *19*, 125606.
(29) Huo, L. H.; Li, Q.; Zhao, H.; Yu, L. J.; Gao, S.; Zhao, J. G. *Sen. Actuators. B* **2005**, *107*, 915.
(30) Scott, R. W. J.; Yang, S. M.; Chabanis, G.; Coombs, N.; Williams, D. E.; Ozin, G. A. *Adv. Mater.* **2001**, *13*, 1468.
(31) Liao, L.; Lu, H. B.; Li, J. C.; He, H.; Wang, D. F.; Fu, D. J.; Liu, C.; Zhang, W. F. *J. Phys. Chem. C* **2007**, *111*, 1900.

JP802968A